

1 **Controls on the Cd-isotope composition of Upper Cretaceous (Cenomanian–**
2 **Turonian) organic-rich mudrocks from south Texas (Eagle Ford Group)**

3

4 Tim C. Sweere^{1,2}, Alexander J. Dickson^{1,3}, Hugh C. Jenkyns¹, Don Porcelli¹, Micha
5 Ruhl^{1,4}, Melissa J. Murphy^{1,5}, Erdem Idiz¹, Sander H.J.M. van den Boorn⁶, James S.
6 Eldrett⁷, and Gideon M. Henderson¹

7

8 **Affiliations:**

9 1. Department of Earth Sciences, University of Oxford, South Parks Road, Oxford,
10 OX1 3AN, UK.

11 2. ETH Zürich, Institute of Geochemistry and Petrology, Department of Earth
12 Sciences, Clausiusstrasse 25, 8092 Zürich, Switzerland.

13 3. Department of Earth Sciences, Royal Holloway University of London, Egham,
14 Surrey, TW20 0EX, UK.

15 4. Department of Geology, Trinity College Dublin, The University of Dublin,
16 Dublin 2, Ireland.

17 5. London Geochemistry and Isotope Centre (LOGIC), University College London,
18 5 Gower Place, London, WC1E 6BS.

19 6. Shell Global Solutions International B.V, Grasweg 31, 1031 HW Amsterdam,
20 the Netherlands.

21 7. Shell Global Solutions International B.V, Kesslerpark 1, 2288 GS Rijswijk, the
22 Netherlands.

23

24 **Abstract**

25

26 The isotopic composition of Cd buried in marine sediments may preserve
27 valuable palaeoenvironmental information on past ocean redox conditions or
28 biological cycling. It is unclear, however, how the Cd-isotope composition of the
29 sedimentary record reflects these processes. In this study, new Cd-isotope data

are presented, along with $\delta^{13}\text{C}$, and Cd, Mo and TOC concentrations, from organic-rich mudrocks from the southern Western Interior Seaway (WIS), spanning the Cenomanian–Turonian stages within the Eagle Ford Group of the Maverick Basin, Texas, USA. Relationships between $[\text{Cd}/\text{TOC}]$, $\delta^{114}\text{Cd}$, and Mo_{EF} indicate that sedimentary Cd was derived from organic matter with additional contributions from CdS formed in euxinic water masses. Local redox conditions exerted a primary control on the $\delta^{114}\text{Cd}$ composition of these deposits, with high $\delta^{114}\text{Cd}$ values attributed to near-quantitative removal from seawater in euxinic environments. Lower $\delta^{114}\text{Cd}$ values in non-euxinic environments may reflect isotopically light Cd associated with organic material due to partial remineralization. These observations imply that $\delta^{114}\text{Cd}$ values of samples deposited in demonstrably euxinic conditions may be used to constrain the $\delta^{114}\text{Cd}_{\text{seawater}}$ coming into the Maverick Basin at this time and give a composition of $0.28 \pm 0.11 \text{ ‰}$ (2 SD) for the Early Cenomanian. Samples from an interval of peak-organic carbon burial globally, namely Oceanic Anoxic Event 2 (OAE 2), show anomalous $\delta^{114}\text{Cd}$ and $[\text{Cd}]$ patterns compared to the rest of the data, implying a perturbation to the dissolved Cd pool. The data presented in this study demonstrate that sedimentary Cd isotopes preserve valuable information on the extent of Cd burial into sulfide-bearing sediments at both local and global scales.

1. Introduction

The distribution of cadmium (Cd) in the modern ocean largely mimics that of the macronutrient phosphorus (e.g. Bruland, 1980; De Baar et al., 1994). A pattern of depleted surface waters and a gradual increase to higher concentrations at depth

is associated with the uptake of Cd by marine primary producers in the surface ocean, and remobilization of Cd at depth upon organic-matter degradation. This typical nutrient-like distribution is observed in most parts of the modern ocean (e.g. Baars et al., 2014; Quay et al., 2015; Middag et al., 2019). It has been suggested that Cd substitutes for zinc in carbonic anhydrase (e.g. Lane et al., 2005), though more recent studies suggest that the majority of Cd uptake is likely non-specific (Horner et al., 2013). The details of Cd uptake mechanisms are still under debate (e.g. Morel, 2013). Regardless, the similarities of Cd and phosphorus distributions in the modern ocean are striking and therefore have led to the suggestion that Cd concentrations in foraminiferal tests (e.g. Boyle, 1988; Elderfield and Rickaby, 2000) and shales (e.g. Brumsack, 2006) may preserve information relating to past oceanic nutrient conditions.

More recently, efforts to map and understand the isotopic composition of dissolved Cd in the modern ocean have revealed a vertical gradient in the surface ocean and a homogeneous deep ocean Cd-isotope composition ($\delta^{114}\text{Cd}$) of $\sim 0.3\text{‰}$ ($\delta^{114}\text{Cd} = [^{114}/^{110}\text{Cd}_{\text{sample}}/^{114}/^{110}\text{Cd}_{\text{NIST}}] - 1) \times 1000$; e.g. Ripperger et al., 2007; Abouchami et al., 2011; Xue et al., 2013; Conway and John, 2015, John et al., 2018). Preferential uptake of the lighter Cd isotopes by primary producers generally leaves the surface ocean strongly enriched in the heavier isotopes (by up to $\sim 5\text{‰}$). This observation is in agreement with Cd-isotope fractionation observed in culture studies (Lacan et al., 2006; Horner et al., 2013; John and Conway, 2014). Other studies have also stressed the importance of lateral transport and global circulation patterns on dissolved Cd-isotope patterns in the modern ocean, with a particularly strong influence by Southern Ocean processes (e.g. Xie et al., 2017; Sieber et al., 2019). The strong biological control on the

dissolved Cd-isotope composition of the modern ocean has led to several studies that explore the use of Cd isotopes as a proxy for past nutrient conditions in carbonates (Hohl et al., 2017; John et al., 2017) and shales (Georgiev et al., 2015).

Cd, however, is generally so highly depleted in surface waters that, to a good approximation, the particles leaving the surface ocean quantitatively remove the element and therefore, on average, have a similar isotope composition to waters added to the surface by upwelling and vertical mixing (Conway and John, 2015; Janssen et al., 2019). Despite this quantitative removal, the isotopic composition of particles in the deeper ocean is generally lower than both the surface ocean particles from which they derive and the dissolved deep-ocean composition, with the lowest values found in the nutricline where a large fraction of sinking particulate Cd becomes remineralized (Janssen et al., 2019). The relatively light isotopic composition of deep particles has been ascribed to either the presence of Cd in multiple particulate pools with different labilities and $\delta^{114}\text{Cd}$ values, or to fractionation during particulate Cd remineralization (Janssen et al., 2019).

The formation of Cd sulfides in the water column and/or pore waters also impacts on Cd cycling in the ocean and sediments. Equilibrium thermodynamics predicts that Cd forms a stable sulfide phase in the presence of free H_2S , rather than being incorporated into pyrite (Al-Farawati & van den Berg, 1999; Morford & Emerson, 1999). Any Cd released to pore waters by the degradation of organic material may therefore be bound in the sediment by the formation of insoluble sulfides (Rosenthal et al., 1995; Little et al., 2015). Cd may also form sulfides in the water column, either in sulfidic micro-environments around degrading organic material in oxygen-deficient zones in the open ocean (Janssen et al.,

2014; Conway and John, 2015) or below the chemocline in stratified, hydrographically restricted basins. Very low Cd concentrations below the chemocline in euxinic (anoxic and sulfidic) waters of the Black Sea and Cariaco Basin suggest near-complete removal of Cd in the latter type of setting (Jacobs and et al., 1987; Tankere et al., 2001). Recent experimental evidence (Guinoisseau et al., 2018) supports inferences from seawater data (Janssen et al., 2014; Conway and John, 2015; Xie et al., 2019) that the $\delta^{114}\text{Cd}$ composition of CdS is isotopically lighter than ambient seawater. Consequently, CdS formation may impact the Cd-isotope composition of the sedimentary record, and potentially exert a significant influence on the global cycling of Cd.

To summarize, modern ocean and laboratory studies indicate three controls on the composition of settling particles and hence primary marine sediment: non-quantitative uptake by primary producers; remineralization of organic material; and non-quantitative CdS formation in the water or sediment. Post-depositional alteration of isotopic signatures may also occur due to remobilization of Cd from organic particles and subsequent non-quantitative CdS formation in pore waters. Diffusion of isotopically light Cd across the sediment-water interface and fixation as CdS may also lead to sedimentary isotopic compositions lower than overlying seawater. Together, these processes lead to Cd-isotope compositions of organic-rich sediments that are either equal to seawater, or lower by as much as $\sim 0.5\text{‰}$ (Bryan, 2019; Little et al., 2019).

This study aims to test whether the isotopic compositions of authigenic Cd preserved in the ancient sedimentary record can be related to palaeoceanographic conditions documented by other more established proxy

approaches. In this context, Cd-isotope data for two drill cores from the Cretaceous Western Interior Seaway of North America are presented. The studied interval hosts Cenomanian–Turonian marls and limestones deposited during a time of dynamic redox and environmental conditions at both local and global scales (e.g. Eldrett et al., 2014, 2015).

2. Geological context

The Upper Cretaceous Eagle Ford Group was deposited on a shallow (100–200 m) carbonate shelf at the southern gateway of the Cretaceous Western Interior Seaway (WIS) and comprises alternating marls and limestones with numerous intercalated volcanic ash beds (Eldrett et al., 2015). Several industry cores have been recovered from the Maverick intra-shelf basin, which allows assessment of the uniformity of stratigraphic $\delta^{114}\text{Cd}$ patterns within a single marine basin (Figure 1). This study is based on two research cores drilled in close proximity to each other in this setting: the Innes-1 core located on the Comanche carbonate shelf, and the Iona-1 core located on the more distal edge of the Maverick intra-shelf basin (Eldrett et al., 2017, Figure 1). Both cores cover roughly the same time interval (98 Ma – 89 Ma), but in the Innes-1 core a considerable (~2 Myr) hiatus is recognized within the Turonian, which has a reduced sedimentary record (representing ~0.2 Myr) in the more distally situated Iona-1 core (Eldrett et al., 2017, Minisini et al., 2018). The Innes-1 and Iona-1 cores include the positive carbon-isotope excursion associated with Oceanic Anoxic Event 2, an interval of globally widespread enhanced organic-carbon burial associated with the spread of low-oxygen marine environments (e.g. Schlanger and Jenkyns,

1976; Scholle and Arthur, 1980; Tsikos et al., 2004; Jenkyns, 2010; Eldrett et al., 2014, 2017). However, the OAE 2 interval is locally characterized by relatively organic-lean deposits, reflecting more oxygenated conditions in the southern WIS (Eldrett et al., 2014). This interval of more oxygenated bottom-water conditions separates the highly organically enriched mudstones of the Lower Eagle Ford Group from the more organic-lean mudstones of the Upper Eagle Ford Group (see Figure 2). Trace-metal concentrations, sedimentary structures, organic biomarkers, and benthic faunal abundances and diversities suggest that the basin was mostly euxinic during deposition of the Lower Eagle Ford, and suboxic to anoxic during deposition of the Upper Eagle Ford (Denne et al., 2014; Eldrett et al., 2014; Sun et al., 2016; Minisini et al., 2018).

3. Methods

3.1 $\delta^{114}\text{Cd}$

Core samples were crushed using an agate pestle and mortar and subsequently treated with inverse *aqua regia* for partial shale digestion. This method has been shown to dissolve authigenic shale components but leaves some detrital minerals intact, and has been successfully used in a previous Cd-isotope study on shales (Georgiev et al., 2014). An aliquot of the digested sample was taken for analysis by ICP-MS to determine Cd concentrations to enable accurate addition of a ^{111}Cd - ^{113}Cd double spike solution. Sample digests were spiked with a ^{111}Cd - ^{113}Cd double spike to obtain a spike:sample ratio of ~ 1 for total Cd, and subsequently separated from major-element cations and isobaric interferences by an anion column chromatography procedure modified from procedures by

Pearce et al. (2009) and Dickson et al. (2016). A summary of the column method is provided in Table 1.

Cd stable-isotope analyses were performed on a Nu Instruments multi-collector ICP-MS at the University of Oxford. Samples were measured at 50 ng g⁻¹ (spike plus sample) concentrations and were bracketed by a spiked NIST-3108 solution to correct for instrumental drift. Data were processed offline using a correction for exponential mass-bias and Sn interference on masses 112 and 114 by analysis of ¹¹⁷Sn. Mass 115 was monitored for possible isobaric interferences by In on mass 113, but In signals were never found to be above background values so no correction was applied. Cd-isotope values are reported as $\delta^{114}\text{Cd}$ relative to NIST-3108, which is defined as $\delta^{114}\text{Cd} = \left[\frac{{}^{114}/{}^{110}\text{Cd}_{\text{sample}}}{{}^{114}/{}^{110}\text{Cd}_{\text{NIST}}} - 1 \right] \times 1000$ (Abouchami et al., 2013). Reported errors in Figure 2 are the standard error propagated uncertainties based on the reproducibility of the bracketing NIST standards and the internal error of sample analysis. The accuracy of Cd-isotope results was estimated by analysis of pure Cd-isotope standards ‘OxCad’ ($-0.86 \pm 0.05 \text{ ‰}$, 2 SD, n = 15); ‘Alpha Cd Zurich’ ($-0.01 \pm 0.06 \text{ ‰}$, 2 SD, n = 8); ‘BAM I012’ ($-1.31 \pm 0.07 \text{ ‰}$, 2 SD, n = 7), which are in agreement with previously published values (Abouchami et al., 2013). External reproducibility is estimated from analyses of rock-standard SDO-1 ($0.13 \pm 0.06 \text{ ‰}$, 2SD, n=5), for which powder aliquots were digested separately in different chemistry batches. The elemental concentrations for the Iona-1 core are from bulk-rock digestion undertaken by Eldrett et al. (2014). The enrichment factors (EF) are defined as $\text{TM}_{\text{EF}} = [\text{TM}/\text{Al}]_{\text{sample}} / [\text{TM}/\text{Al}]_{\text{crust}}$ with upper continental crust values of $[\text{Cd}/\text{Al}]_{\text{crust}} = 0.011 \times 10^{-4}$ and $[\text{Mo}/\text{Al}]_{\text{crust}} = 0.13 \times 10^{-4}$ after

Rudnick and Gao (2003). Cd concentrations of the 'carbonate-free' fraction are calculated as $[Cd]_{\text{carb-free}} = [Cd] / (1 - [CaCO_3])$.

3.2 $\delta^{13}C$

New bulk-rock organic $\delta^{13}C$ ($\delta^{13}C_{\text{TOC}}$) analysis was performed on 329 samples from the Iona-1 core, spanning the entire Lower Eagle Ford and the lower part of the Upper Eagle Ford, including the Cenomanian–Turonian transition and the positive carbon-isotope excursion (CIE) associated with the OAE 2 event. One gram of homogenized sample was treated with 40mL of 1 M cold HCl to dissolve sedimentary carbonate. Samples (dissolved in 1 molar HCl) were then put on a hot plate for 4 hours at $\sim 80^\circ\text{C}$, rinsed 4 times with distilled water to reach neutral pH, and finally oven-dried (at 30°C) and again powdered. Around 1–15mg (depending on organic-carbon content) of homogenized de-carbonated sample residue was weighed into an 8×5-mm tin capsule for $\delta^{13}C_{\text{TOC}}$ analyses.

Bulk organic-carbon isotope analysis was performed at the School of Archaeology, University of Oxford, using a Carlo Erba Elemental Analyzer coupled to a Europa Geo 20–20 IRMS, and at the Stable Isotope Laboratory of the Open University (Milton Keynes, UK), with a Thermo Scientific Flash 2000 HT Elemental Analyzer (EA) coupled to a Thermo Scientific MAT253 isotope-ratio mass spectrometer via a ConFlo IV open split interface. The Thermo Scientific Flash 2000 HT EA has a MAS2000 carousel and between the carousel and the EA sits a Thermo No Blank Device (NBD), allowing for the single sample purging with helium. The EA is also equipped with a Thermal Conductivity Detector (TCD). Automated dilution of sample gas with the ConFlo IV open split interface allows for high dynamic range of C+N content and controlled the introduction of

the “reference” gases.

Analytical precision was checked with the routine analysis of four internal and referenced laboratory standards (urea 020914MAG, IAEA-CH-6, NIST 8573, IRR041), showing measured average $\delta^{13}\text{C}$ values of -45.24‰, -10.39‰, -26.52‰, -23.58‰, respectively, and standard deviations of 0.85‰, 0.12‰, 0.28‰, 0.49‰. Regular analyses of 45 alanine-standards, in between samples, showed average $\delta^{13}\text{C}$ values of -26.92‰, with a standard deviation of 0.22‰. An internal nylon standard ($\delta^{13}\text{C} = -26.16\text{‰} \pm 0.21$) was used for analytical reference analysis. Isotope ratios are reported in standard delta notation relative to Vienna PDB. The new data are here combined with the previously published data from Eldrett et al., (2014), into a composite Iona-1 $\delta^{13}\text{C}_{\text{TOC}}$ record with significantly increased stratigraphical resolution of, on average, every ~13cm (Figures 2 and 7). This dataset now covers all sedimentary facies, across the metre-scale marl–limestone couplets, and across the studied interval of environmental change.

4. Results

All samples are significantly enriched in Cd relative to the composition of the average upper continental crust. Enrichment factors (Cd_{EF}) range from 2.4 to 314 with an average of 66 ($n = 27$) for the Iona-1 core and from 3.8 to 131 with an average of 54 ($n = 18$) for the Innes-1 core. The average proportion of detrital Cd in these rocks is 5%, with a maximum of 41% for some outliers, based on the average composition of upper continental crust given by Rudnick and Gao (2003) and Al abundances from Eldrett et al. (2014) or this study (see

supplementary info). However, the contribution of Cd from detrital minerals on the Cd-isotope values will be much lower than this, as the Cd-isotope data are based on the partial *aqua regia* digestions. Therefore, no correction for the lithogenic component of Cd in these sediments was performed on $\delta^{114}\text{Cd}$.

Sediment $\delta^{114}\text{Cd}$ values vary between -0.17 and 0.39 ‰ with an average of 0.15 ± 0.26 ‰ (2 SD, n = 39) for the Iona-1 core and between -0.18 and 0.41‰ with an average of 0.17 ± 0.27 (2 SD, n = 25) for the Innes-1 core. Average $\delta^{114}\text{Cd}$ values are thus similar for the two cores. A comparison between the two cores also highlights similarities in stratigraphic $\delta^{114}\text{Cd}$ patterns (Figure 2). The highest values ($\sim 0.3\text{--}0.4$ ‰) are generally found in deposits of the lowermost part of the Lower Eagle Ford Group, which are characterized by high levels of organic-matter enrichment, whereas the lowest values ($-0.1\text{--}0.1$ ‰) are found over the OAE 2 interval, locally characterized by the most organic-lean sediments and a positive $\delta^{13}\text{C}$ excursion. In both cores, $\delta^{114}\text{Cd}$ values for the Upper Eagle Ford Group ($\sim 0.1\text{--}0.2$ ‰) are mostly slightly lower than those of the Lower Eagle Ford Group, but higher than those recorded during the OAE. Smaller scale $\delta^{114}\text{Cd}$ excursions to lighter values also occur during other stratigraphic intervals with positive carbon-isotope excursions: namely, the Mid-Cenomanian Event, Jukes-Browne Event, Pewsey and Hitch Wood excursions (Jarvis et al., 2006; Joo and Sageman, 2014; Eldrett et al., 2017).

Mo data come from Eldrett et al. (2014) for the Iona-1 core with additional data generated for the Innes-1 core in this study, and were measured on the same samples as the Cd data. Mo enrichment factors (Mo_{EF}) range from 1.7 to 1009 with an average of 156 (n = 48) for the Iona-1 core and from 1.8 to 315 with an average of 102 (n = 19) for the Innes-1 core.

279 The composite high-resolution $\delta^{13}\text{C}_{\text{TOC}}$ record from the Iona-1 core,
280 combining the previously published data from Eldrett et al. (2014) and the new
281 data reported here, shows a significant 3–4‰ positive excursion, from
282 Cenomanian (Lower Eagle Ford) $\delta^{13}\text{C}_{\text{TOC}}$ background values of -27 to -28 ‰.
283 This shift across the Lower to Upper Eagle Ford transition reflects the globally
284 recognized interval of OAE 2 (Figure 2). In detail, the carbon-isotope profile, in
285 common with similar patterns elsewhere, shows an initial rise, conventionally
286 taken to mark the base of the OAE interval, followed by a fall-back, in turn
287 followed by a sustained rise into the so-called plateau phase that shows high
288 $^{13}\text{C}_{\text{TOC}}$ values (cf. Tsikos et al., 2004).

289 The OAE 2 positive CIE is followed by a reduction in $\delta^{13}\text{C}_{\text{TOC}}$ values to ~-
290 26 ‰ in the lowermost Turonian, followed by a further decrease down to ~-27
291 ‰ in the middle Turonian (Upper Eagle Ford; Figure 2). Superimposed on the
292 long-term trend in $\delta^{13}\text{C}_{\text{TOC}}$, smaller and stratigraphically shorter positive carbon-
293 isotope excursions of 1–3 ‰ can be recognized in the Cenomanian (the Mid-
294 Cenomanian Event (MCE) and the Jukes Browne Event) and the Turonian (the
295 Pewsey and Hitchwood Events) parts of the Eagle Ford succession (Figure 2).
296 Combined with the published biostratigraphic and geochronological constraints
297 on the studied Iona-1 core, this new chemostratigraphic framework allows for
298 detailed correlation to records elsewhere.

299 $\delta^{13}\text{C}_{\text{TOC}}$ data for the Innes-1 core (Eldrett et al., 2017) shows the
300 characteristic positive excursion of ~4‰ associated with the OAE 2 event
301 during the Cenomanian–Turonian boundary interval as described above in more
302 detail for the Iona-1 core. Positive C-isotope excursions have also been
303 recognized for other intervals in this core and have been linked been to the Mid-

Cenomanian and Pewsey events also found in the calcite composite record (Jarvis et al., 2006; Eldrett et al., 2017).

5 Discussion

5.1 Causes of sedimentary Cd enrichments

For a mechanistic understanding of the stratigraphic changes in $\delta^{114}\text{Cd}$ compositions it is important to address how Cd was incorporated into the sediments. The concentration of Cd can be compared to total organic carbon (TOC) and Mo enrichment factors (Mo_{EF}) to provide insight as to whether the Cd is associated with organic or sulfide fractions (Figure 3). Molybdenum (Mo) in marine sediments is a well-established proxy for local redox conditions and is enriched in sediment when increasingly sulfidic conditions promote the formation of thiomolybdate, polysulfide and/or Fe-S-Mo species (e.g. Erickson and Helz, 2000; Scott and Lyons, 2012).

Cd is positively correlated to TOC with a range of different Cd/TOC values (Figure 3). Sediments without significant Mo enrichment (i.e. $\text{Mo}_{\text{EF}} < 25$) have a range of Cd/TOC from 0.065 to 0.28 (denoted by the grey shaded region in Figure 3), with one exception of 0.65. This range of Cd/TOC is similar to values inferred for exported particles in non-HNLC (high-nutrient low chlorophyll) regions based on dissolved Cd and P patterns (Quay et al., 2015) and to values found in modern marine biota in culture studies (Ho et al., 2003; Figure 3). Therefore, while Cd uptake by phytoplankton can vary considerably as a function of nutrient availability (e.g. Bourne et al., 2018), this comparison suggests that most of the Cd in these samples was associated with uptake in biological

material. By contrast, all samples which are noticeably enriched in Mo ($\text{Mo}_{\text{EF}} > 100$) have higher Cd/TOC ratios than most modern marine biota, suggesting that they have formed in euxinic conditions and, in addition to Cd in organic material, have incorporated Cd by precipitation of CdS in euxinic conditions. The supply of Cd to the basin must have been high enough to sustain high Cd/TOC values for these intervals (e.g. Algeo and Lyons, 2006).

5.2. Controls on $\delta^{114}\text{Cd}$

Local redox conditions also represent the dominant control on $\delta^{114}\text{Cd}$ values, as implied by a positive relationship between $\delta^{114}\text{Cd}$ and Mo_{EF} (Figure 4). High Mo enrichments and Cd/TOC values, indicative of euxinic conditions, correspond to the highest $\delta^{114}\text{Cd}$ values. By contrast, more oxygenated conditions result in lower Mo_{EF} and Cd/TOC, and a tendency toward lower $\delta^{114}\text{Cd}$ values. It is likely that the high $\delta^{114}\text{Cd}$ values in euxinic sediments reflect near-quantitative removal of Cd from the seawater to the sediment through the formation of authigenic CdS in euxinic conditions (coupled to the minimal remineralization of organic matter). Under such conditions, the $\delta^{114}\text{Cd}$ is likely to have equalled that in the local overlying seawater. Similar observations have been made for Zn in modern sediment data from the euxinic basins of the Cariaco Basin and Black Sea, where sediments reflect the Zn-isotope composition of the deep ocean (Vance et al., 2016; Isson et al, 2018).

Several mechanisms could explain the observation of lower $\delta^{114}\text{Cd}$ values in non-euxinic conditions (see Figure 5 for a conceptual summary). Delivery of Cd to the sediment in these non-euxinic conditions would have predominantly occurred in sinking organic material (section 5.1). For the organic particles

reaching the sediment to be isotopically lighter than overlying seawater requires either that Cd uptake in the surface ocean was non-quantitative, or that remineralization of some of the organic matter during settling led to preferential release of isotopically heavy Cd (as seen in the modern North Pacific by Janssen et al. 2019). These two mechanisms cannot be distinguished for these Eagle Ford samples with the present data, but the fact that modern sediments have $\delta^{114}\text{Cd}$ lower than seawater by a similar magnitude as that observed in this study (Bryan, 2019; Little et al., 2019), despite today's quantitative biological uptake of Cd in the surface ocean, suggests that the remineralization pathway is important. Due to the variable Cd/P ratios in modern marine phytoplankton (e.g. Bourne et al., 2018), the relative contribution of Cd by organic *versus* sulphide fractions cannot be accurately constrained. The isotopic composition of the organically bound Cd can therefore not be estimated from the data presented here.

An additional mechanism to explain the isotopically light Cd values in non-euxinic sediments may be non-quantitative removal of Cd into CdS forming at depth in the sediment. Breakdown of organic material in the sediment could have released Cd, some of which was incorporated into CdS near to the sulfate-reduction front, with diffusion of the heavier Cd isotopes back to seawater (Guinoisseau et al., 2018).

5.3 Explaining stratigraphic variation in $\delta^{114}\text{Cd}$ and constraints on $\delta^{114}\text{Cd}_{\text{seawater}}$

The control of local redox conditions on sedimentary $\delta^{114}\text{Cd}$ values can explain much of its stratigraphic variability, particularly the difference between the largely non-euxinic Upper Eagle Ford and euxinic Lower Eagle Ford Group (Figure 2; Eldrett et al., 2014; Sun et al., 2016).

Flattening of the relationship between Mo enrichments and $\delta^{114}\text{Cd}$ for $\text{Mo}_{\text{EF}} > 150$ (Figure 4) implies that samples with higher Mo enrichments reflect the quantitative removal of Cd from seawater. These samples may therefore be used to constrain the value of the local seawater $\delta^{114}\text{Cd}$ in the Maverick Basin at that time. The observed value of $0.28 \pm 0.11 \text{ ‰}$ (2 SD, $n=13$), is comparable to the modern deep ocean (e.g. Ripperger et al., 2007; Xue et al., 2013; Conway and John, 2015, John et al., 2018) though it is not known whether or not the water in the Maverick Basin represents the global ocean at this time, or an isotopically evolved water mass sourced from the near-surface proto-North Atlantic Ocean or the northern WIS.

The shallow depth of the Maverick Basin (100–200 m) implies that waters flowing into it would likely have been sourced either from (presumably) isotopically heavy near-surface waters of the proto-North Atlantic Ocean, or from deep-water upwelling or local inputs. The $\delta^{114}\text{Cd}$ value of $0.28 \pm 0.11 \text{ ‰}$ (2 SD), inferred for the Cd-isotope composition of waters coming into the basin, therefore requires that (1) the Cd-isotopic composition of the global deep ocean was $<0.28 \text{ ‰}$ during the Early Cenomanian and thereby isotopically lighter than the modern ocean, or (2) local sources of Cd were significant, or (3) upwelling of deep Tethyan waters was the major source of Cd to the Maverick Basin. The latter option is possible, considering the position of the basin at the southern edge of the Western Interior Seaway, in proximity to the Tethys, with its inferred associated inflow of Tethyan waters, for most of the studied interval (Eldrett et al., 2017). However, significant input of local sources cannot be excluded given the position of the Maverick Basin in a shallow sea. With the current data, it is not possible to further constrain the Cd-isotope composition of waters coming

into the basin. These data therefore do not allow a clear assessment of temporal evolution of the Cd-isotopic composition of the global ocean.

Although the lowest $\delta^{114}\text{Cd}$ values observed in this study for all samples (-0.18‰) are $\sim 0.5\text{‰}$ lower than these reconstructed $\delta^{114}\text{Cd}_{\text{seawater}}$ values, the typical offset for most samples is $< 0.3\text{‰}$. These values are similar to the maximum and average difference between modern seawater and sediments underlying non-euxinic water columns (Bryan, 2019; Little et al., 2019). A cross-plot of the Cd-isotope composition with the inverse of the Cd concentration illustrates different sedimentary end-members that reflect CdS after quantitative removal (i.e. the 'seawater component') and isotopically lighter Cd associated with the organic flux under non-euxinic conditions. Sediments formed during the carbon-isotope plateau phase of OAE 2 are significant outliers, exhibiting substantially lower Cd concentrations for a given Cd-isotopic ratio (Figure 6).

5.4 The OAE 2 interval

Samples from the OAE 2 interval show anomalously low Cd concentrations and fall away from the $\delta^{114}\text{Cd}$ versus $1/\text{Cd}$ relationship visible for other intervals (Figure 6). Major changes in local redox conditions cannot directly explain the anomalously low Cd concentrations for this interval. Local oxygenation apparently mostly took place just prior to the onset of the OAE 2 interval, as evidenced by a drop in Mo_{EF} (Figure 7). This redox change from euxinic to non-euxinic conditions was associated with a decrease in $\delta^{114}\text{Cd}$, Cd concentrations, and Cd/TOC, and falls within the general sample population as described in the section 5.3. Mo enrichment factors are relatively low and constant stratigraphically upward from this initial drop, indicating non-euxinic

conditions. $\delta^{114}\text{Cd}$ values, however, gradually rise following the local oxygenation and are accompanied by a further drop in Cd concentrations relative to TOC. The gradual increase in $\delta^{114}\text{Cd}$ and anomalously low Cd concentrations therefore cannot directly be explained by locally changing redox conditions.

Changes to the dissolved Cd pool coming into the basin could, however, explain the observed patterns, with lower dissolved Cd concentrations and a gradual rise in dissolved $\delta^{114}\text{Cd}$ values. The carbon-isotope excursion signifies the enhanced burial of ^{12}C in organic-rich sediments at a global scale, where the highest values represent peak organic-carbon burial globally (e.g. Scholte and Arthur, 1980; Schlanger et al., 1987). Burial of isotopically light Cd in these organic-rich sediments could explain the inferred change to an isotopically heavier global dissolved Cd pool with lower Cd concentrations during the positive carbon-isotope excursion. Anomalously low concentrations (relative to TOC) of other trace metals (e.g. Mo, Zn) have been found in previous studies for the OAE 2 event interval in other locations and were linked to the global drawdown of the dissolved pool of these elements (e.g. Hetzel et al., 2009; Owens et al., 2016, Dickson et al., 2016; 2017).

Considering that the sediments of the Maverick Basin were deposited in a shallow sea, regional changes in watermass circulation or relative sea level could potentially also have impacted $\delta^{114}\text{Cd}_{\text{seawater}}$ and supply of dissolved Cd. The OAE 2 interval is associated with a time of maximum flooding of the southern WIS and the temporary incursion of boreal waters into the Maverick Basin (Eldrett et al., 2017 Minisini et al., 2018). Removal of Cd by primary producers during the long transfer over the shallow seas of the WIS may explain relatively low [Cd] for

the putative boreal water mass supplied to the basin during this interval. Maximum flooding of the southern WIS could generally be expected to have allowed deeper, and therefore isotopically lighter waters with higher Cd concentrations to flow into the basin. Sea-level change is therefore not considered a likely explanation for lower [Cd] or gradually rising $\delta^{114}\text{Cd}_{\text{seawater}}$.

However, such interpretations remain speculative, as absolute $\delta^{114}\text{Cd}_{\text{seawater}}$ values for this interval cannot be constrained with reasonable confidence due to the unknown size of the offset between sediments and seawater in non-euxinic environments. Any assessment of a global perturbation to the Cd cycle associated with major palaeoenvironmental change in future studies should focus on the study of settings with relatively constant local redox conditions or Cd-isotope analysis on specific sediment phases.

6 Conclusions

- Stratigraphic patterns in sedimentary [Cd] and $\delta^{114}\text{Cd}$ are reproducible between two Upper Cretaceous cores through the Eagle Ford Group in the southern Western Interior Seaway Maverick Basin, and vary with key changes in other palaeoenvironmental parameters.
- By comparison of [Cd] with TOC and Mo_{EF} in the sediments, two sources of sedimentary Cd are identified. A significant fraction was delivered in organic matter, with an additional source from CdS precipitation when water masses were euxinic.
- The relationships of Cd isotopes with TOC and Mo_{EF} implies that local redox conditions exerted a primary control on the $\delta^{114}\text{Cd}$ composition of these sediments.

- Non-euxinic conditions record lower $\delta^{114}\text{Cd}$ values, probably due to partial remineralization of sinking particles. Alternative explanations for lower $\delta^{114}\text{Cd}$ values in more oxygenated conditions are isotope fractionation associated with the non-quantitative uptake of Cd in the surface ocean or the non-quantitative precipitation of CdS in sulfidic pore waters.
- Euxinic conditions led to the near-quantitative removal of Cd as CdS, such that sediments likely record local $\delta^{114}\text{Cd}_{\text{seawater}}$ values in the Maverick Basin at that time. This approach constrains local $\delta^{114}\text{Cd}_{\text{seawater}}$ values for the Maverick Basin to have been $0.28 \pm 0.11 \text{ ‰}$ (2SD) for much of the Cenomanian interval.
- Cd concentrations and $\delta^{114}\text{Cd}$ values for the OAE 2 interval do not follow general patterns as observed for other parts of the Iona-1 and Innes-1 cores, which may be the result of a perturbation to the dissolved Cd pool, like the global drawdown of Cd or changes in regional circulation patterns.
- This study clearly illustrates the need to consider local redox conditions before relating sedimentary Cd isotope values to global geochemical change.

Acknowledgements

We thank Shell Global Solutions International B.V. for access to samples and financial support, Daniel Minisini and Steve Bergman for their input at an early stage of this project, and three anonymous reviewers for their constructive comments on the manuscript.

Figure captions

Figure 1: (A) Palaeogeographical reconstruction of the Cenomanian–Turonian Boundary interval with approximate study locations, modified from Jarvis et al. (2011). (B) Schematic reconstruction of basin characteristics for the Maverick Basin, modified from Eldrett et al. (2017). The water depth estimate comes from Eldrett et al. (2015), and is based on the observation that most sediments were deposited below wave-base. The areas marked with CLIP and HALIP reflect the position of the Caribbean and High Arctic Large Igneous Provinces, respectively.

Figure 2: (A) Cd-isotope stratigraphy for the Innes-1 and Iona-1 cores. Horizontal red bands mark recognized intervals of positive carbon-isotope excursions. The right-hand column represents general redox conditions as inferred from previous studies on trace-metal and organic geochemistry (Eldrett et al., 2014; Sun et al., 2016). The $\delta^{13}\text{C}_{\text{org}}$ and TOC data are from Eldrett et al. (2014), Scaife et al. (2017), with additional, new $\delta^{13}\text{C}_{\text{org}}$ data presented here to increase stratigraphic resolution for the Iona-1 core. The Mo (EF) data for the Iona-1 core are from Eldrett et al. (2014). (B) Comparison of Cd-isotope data for both cores, plotted against ages of Eldrett et al. (2017).

524

525 Figure 3: Cd concentrations compared to Total Organic Carbon (TOC)
526 concentrations. The solid line denoting 'non-HNLC' (high-nutrient low-
527 chlorophyll) represents the Cd/P ratios estimated for exported particles in non-
528 HNLC ratios based on dissolved Cd and P patterns of Cd/P = 0.21 mmol/mol
529 (Quay et al., 2015). This value is identical to average compositions of cultured
530 phytoplankton species reported by Ho et al. (2003). Although it should be noted
531 that Cd/P values vary considerably in the modern ocean (e.g. Bourne et al.,
532 2018), the Cd/P value of 0.21 shown here provides a reasonable general
533 indication of organic-bound Cd as estimated from both dissolved Cd/P patterns
534 in non-HNLC regions and from culture studies. Cd/P values were converted to
535 Cd/TOC assuming a P:C ratio of 1:124 (Ho et al., 2003). The grey shading
536 between the dashed lines includes, with one exception, all samples with $Mo_{EF} <$
537 25, reflecting dominantly non-euxinic conditions.

538

539 Figure 4. $\delta^{114}Cd$ relative to Mo_{EF} and Cd/TOC. The positive relationships
540 observed are suggested to have been caused by the quantitative and non-
541 quantitative removal of dissolved Cd into sediments in euxinic and non-euxinic
542 environments, respectively. The dashed line at $Mo_{EF} = 150$ indicates the
543 flattening of the curve and is later used to constrain local $\delta^{114}Cd_{seawater}$ values.

544

545 Figure 5. Simplified conceptual summary of processes considered to control
546 sedimentary $\delta^{114}Cd$ values in non-euxinic *versus* euxinic environments. Black
547 arrows reflect cycling and contribution of organically bound Cd to the sediment,
548 whereas the white reflect the contribution by CdS (1) $\delta^{114}Cd$ values of surface

ocean particulates are generally not expected to be fractionated from source values due to quantitative removal of dissolved Cd in the surface ocean (e.g. Conway and John, 2015; Janssen et al., 2019). Non-quantitative removal in specific cases could potentially leave the surface-ocean particles isotopically lighter than deep waters (2) Cd remineralization in the water column causes the $\delta^{114}\text{Cd}$ values of sinking organic particles to be lower than deep-ocean values (Janssen et al., 2019). This effect is expected to be smaller in strongly reducing conditions due to considerably lower remineralization rates, such that the $\delta^{114}\text{Cd}$ values of sinking organic particles approach those of surface ocean particles, and thus approach input values (3) Non-euxinic environments may allow the preferential uptake of isotopically light Cd as CdS in sulfidic pore waters. A largely sulfidic water column would be expected to lead to the near-quantitative removal of Cd from the water column as CdS, so that $\delta^{114}\text{Cd}_{\text{sediment}}$ approaches the Cd-isotope composition of input to the basin. (4) In sediments from euxinic environments, the proportion of total Cd associated with CdS is higher due to CdS formation in the water column, in contrast to non-euxinic conditions where most Cd is supplied as part of sinking organic particles.

Figure 6. (A) $\delta^{114}\text{Cd}$ relative to the inverse of the carbonate-free Cd concentration. This presentation highlights possible mixing of different phases as they would appear as linear relationships. The black symbols indicate samples with $\text{Mo}_{\text{EF}} > 150$, taken to represent the local Cd-isotope composition of basin input. Outliers with anomalously low Cd concentrations are mostly from the plateau phase of the carbon-isotope excursion associated with the OAE 2 event, as bracketed by the highest $\delta^{13}\text{C}_{\text{org}}$ values in (B). Considering the highly variable

CaCO₃ content in these samples (e.g. Eldrett et al., 2017), Cd concentrations are presented as [Cd]_{carb-free}.

Figure 7: Patterns in $\delta^{114}\text{Cd}$ and supporting variables for the Iona-1 core plotted for an interval from 125 to 70m depth that includes the OAE 2 interval. The yellow band highlights an interval of major local redox change based on Mo_{EF} values, whereas the horizontal dashed lines bracket an interval with anomalously low Cd concentrations, relative to TOC.

583 Table 1. Cd separation and purification chemistry

584

First stage: 2mL AG1X-8 anion exchange resin (200–400 mesh)

Eluent	Quantity (mL)	Purpose
7.5 M HNO ₃	10	resin cleaning
MQ Ultrapure water	2	rinse
6 M HCl	10	resin cleaning
1 M HCl	30	resin cleaning
1 M HF / 0.5 M HCl	4	resin conditioning
1 M HF / 0.5 M HCl	6	elute matrix (majors, In)
sample solution		
1 M HF / 0.5 M HCl	8	elute matrix (majors, In)
4 M HCl	8	elute matrix (Zr)
3 M HNO ₃ / 0.1 M HBr	12	elute matrix (Mo, Sn)
3 M HNO ₃	7	elute Cd

Second stage: 200 µL AG1X-8 anion exchange resin (200–400 mesh)

Eluent	Quantity (mL)	Purpose
7.5 M HNO ₃	1	resin cleaning
MQ Ultrapure water	0.2	rinse
6 M HCl	1	resin cleaning
1 M HCl	3	resin cleaning
1 M HF / 0.5 M HCl	0.4	resin conditioning
1 M HF / 0.5 M HCl	0.6	elute matrix (majors, In)
sample solution		

1 M HF / 0.5 M HCl	1.2	elute matrix (majors, In)
4 M HCl	1	elute matrix (Zr)
3 M HNO ₃ / 0.1 M HBr	1	elute matrix (Mo, Sn)
3 M HNO ₃	1	elute Cd

585

586

References

- Abouchami, W., Galer, S. J., Horner, T. J., Rehkämper, M., Wombacher, F., Xue, Z., Lambelet, M., Gault-Ringold, M., Stirling, C. H., & Schönbachler, M. (2013). A common reference material for cadmium isotope studies–NIST SRM 3108. *Geostandards and Geoanalytical Research*, **37**, 5–17.
- Abouchami, W., Galer, S., De Baar, H., Alderkamp, A., Middag, R., Laan, P., Feldmann, H., & Andreae, M. (2011). Modulation of the southern ocean cadmium isotope signature by ocean circulation and primary productivity. *Earth and Planetary Science Letters*, **305**(1), 83–91.
- Al-Farawati, R. & van den Berg, C. M. (1999). Metal–sulfide complexation in seawater. *Marine Chemistry*, **63**, 331–352.
- Algeo, T. J., & Lyons, T. W. (2006). Mo–total organic carbon covariation in modern anoxic marine environments: Implications for analysis of paleoredox and paleohydrographic conditions. *Paleoceanography*, **21**(1).
- de Baar, H. J., Saager, P. M., Nolting, R. F., & van der Meer, J. (1994). Cadmium versus phosphate in the world ocean. *Marine Chemistry*, **46**, 261–281.
- Baars, O., Abouchami, W., Galer, S. J., Boye, M., & Croot, P. L. (2014). Dissolved cadmium in the southern ocean: distribution, speciation, and relation to phosphate. *Limnology and Oceanography*, **59**, 385–399.

612

613 Boyle, E. A. (1988). Cadmium: Chemical tracer of deepwater paleoceanography.
 614 *Paleoceanography*, **3**, 471–489.

615

616 Bourne, H. L., Bishop, J. K. B., Lam, P. J., & Ohnemus, D. C. (2018). Global spatial
 617 and temporal variation of Cd: P in euphotic zone particulates. *Global*
 618 *Biogeochemical Cycles*, **32** (7), 1123–1141.

619

620 Bruland, K. W. (1980). Oceanographic distributions of cadmium, zinc, nickel, and
 621 copper in the north pacific. *Earth and Planetary Science Letters*, **47**, 176–198.

622

623 Brumsack, H.-J. (2006). The trace metal content of recent organic carbon-rich
 624 sediments: implications for cretaceous black shale formation. *Palaeogeography,*
 625 *Palaeoclimatology, Palaeoecology*, **232**, 344–361.

626

627 Bryan, A. (2019). Investigation of the controls on the cadmium isotope
 628 composition of modern marine sediments. *DPhil thesis, University of Oxford*.

629

630 Conway, T. M. & John, S. G. (2015). Biogeochemical cycling of cadmium isotopes
 631 along a high-resolution section through the north Atlantic Ocean. *Geochimica et*
 632 *Cosmochimica Acta*, **148**, 269–283.

633

634 Denne, R.A., Hinote, R.E., Breyer, J.A., Kosanke, T.H., Lees, J.A., Engelhardt-Moore,
 635 N., Spaw, J.M. and Tur, N. (2014), The Cenomanian–Turonian Eagle Ford Group of
 636 South Texas: insights on timing and paleoceanographic conditions from

637 geochemistry and micropaleontologic analyses. *Palaeogeography,*
638 *Palaeoclimatology, Palaeoecology*, **413**, 2–28.

639

640 Dickson, A.J., Saker-Clark, M., Jenkyns, H.C., Bottini, C., Erba, E., Russo, F.,
641 Gorbanenko, O., Naafs, B.D.A., Pancost, R.D., Robinson, S.A., van den Boorn,
642 S.H.J.M. and Idiz, E. (2017), A southern hemisphere record of global trace-metal
643 drawdown and orbital modulation of organic-matter burial across the
644 Cenomanian–Turonian boundary (Ocean Drilling Programme Site 1138,
645 Kerguelen Plateau). *Sedimentology*, **64**, 186–203.

646

647 Dickson A.J., Jenkyns H.C., Porcelli D., van den Boorn S., and Idiz E. (2016) Basin-
648 scale controls on the molybdenum-isotope composition of seawater during
649 Oceanic Anoxic Event 2 (Late Cretaceous). *Geochimica et Cosmochimica Acta*,
650 **178**, 291–306.

651

652 Elderfield, H. & Rickaby, R.E.M. (2000). Oceanic Cd/P ratio and nutrient
653 utilization in the glacial Southern Ocean. *Nature*, **405**, 305–310.

654

655 Erickson, B. E. & Helz, G. R. (2000). Molybdenum (VI) speciation in sulfidic
656 waters: stability and lability of thiomolybdates. *Geochimica et Cosmochimica*
657 *Acta*, **64**, 1149–1158.

658

659 Eldrett J.S., Minisini D., and Bergman S.C. (2014) Decoupling of the carbon cycle
660 during Ocean Anoxic Event 2. *Geology*, **42**, 567–570.

661

662 Eldrett, J.S., Ma, C., Bergman, S.C., Lutz, B., Gregory, F.J., Dodsworth, P., Phipps, M.,
 663 Hardas, P., Minisini, D., Ozkan, A., Ramezani, J., Bowring, S.A., Kamo, S.L.,
 664 Macaulay, C. and Kelly, A. (2015), An astronomically calibrated stratigraphic of
 665 the Cenomanian, Turonian and earliest Coniacian from the Cretaceous Western
 666 Interior Seaway, USA: implications for global chronostratigraphy. *Cretaceous*
 667 *Research*, **56**, 316–344.
 668
 669 Eldrett, J.S., Dodsworth, P., Bergman, S.C., Wright, M. and Minisini, D. (2017),
 670 Water-mass evolution in the Cretaceous Western Interior Seaway of North
 671 American and equatorial Atlantic. *Climate of the Past*, **13**, 855–878.
 672
 673 Georgiev, S. V., Horner, T. J., Stein, H. J., Hannah, J. L., Bingen, B., & Rehkämper, M.
 674 (2015). Cadmium-isotopic evidence for increasing primary productivity during
 675 the Late Permian anoxic event. *Earth and Planetary Science Letters*, **410**, 84–96.
 676
 677 Guinoiseau, D., Galer, S. J., & Abouchami, W. (2018). Effect of cadmium sulphide
 678 precipitation on the partitioning of Cd isotopes: Implications for the oceanic Cd
 679 cycle. *Earth and Planetary Science Letters*, **498**, 300–308.
 680
 681 Hetzel, A., Böttcher, M. E., Wortmann, U. G., & Brumsack, H. J. (2009). Paleo-redox
 682 conditions during OAE 2 reflected in Demerara Rise sediment geochemistry
 683 (ODP Leg 207). *Palaeogeography, Palaeoclimatology, Palaeoecology*, **273**(3-4),
 684 302–328.
 685

686 Ho, T. Y., Quigg, A., Finkel, Z. V., Milligan, A. J., Wyman, K., Falkowski, P. G., &
687 Morel, F. M. (2003). The elemental composition of some marine phytoplankton.
688 *Journal of phycology*, **39**(6), 1145–1159.

689

690 Hohl, S., Galer, S., Gamper, A., & Becker, H. (2017). Cadmium isotope variations in
691 neoproterozoic carbonates—a tracer of biologic production? *Geochemical*
692 *Perspectives Letters*, **3**, 32–44.

693

694 Horner, T. J., Lee, R. B., Henderson, G. M., & Rickaby, R. E. (2013). Nonspecific
695 uptake and homeostasis drive the oceanic cadmium cycle. *Proceedings of the*
696 *National Academy of Sciences*, **110**, 2500–2505.

697

698 Isson, T. T., Love, G. D., Dupont, C. L., Reinhard, C. T., Zumberge, A. J., Asael, D., ... &
699 Rainbird, R. H. (2018). Tracking the rise of eukaryotes to ecological dominance
700 with zinc isotopes. *Geobiology*, **16**(4), 341–352.

701

702 Jacobs, L., Emerson, S., & Huested, S. S. (1987). Trace metal geochemistry in the
703 Cariaco Trench. *Deep Sea Research Part A. Oceanographic Research Papers*, **34**(5-
704 6), 965–981.

705

706 Janssen, D. J., Conway, T. M., John, S. G., Christian, J. R., Kramer, D. I., Pedersen, T.
707 F., & Cullen, J. T. (2014). Undocumented water column sink for cadmium in open
708 ocean oxygen-deficient zones. *Proceedings of the National Academy of Sciences*,
709 **111**, 6888–6893.

710

711 Janssen, D. J., Abouchami, W., Galer, S. J., Purdon, K. B., & Cullen, J. T. (2019).
712 Particulate cadmium stable isotopes in the subarctic northeast Pacific reveal
713 dynamic Cd cycling and a new isotopically light Cd sink. *Earth and Planetary*
714 *Science Letters*, **515**, 67–78.

715

716 Jarvis, I., Gale, A.S., Jenkyns, H.C. & Pearce, M.A. (2006), Secular variation in late
717 Cretaceous carbon isotopes: a new $\delta^{13}\text{C}$ carbonate reference curve for the
718 Cenomanian–Campanian (99.6–70.6 Ma). *Geological Magazine*, **143**, 561–608.

719

720 Jarvis, I., Lignum, J. S., Gröcke, D. R., Jenkyns, H. C. & Pearce, M. A. (2011). Black
721 shale deposition, atmospheric CO_2 drawdown, and cooling during the
722 Cenomanian-Turonian oceanic anoxic event. *Paleoceanography*, **26**. PA3201,
723 doi:10.1029/2010PA002081.

724

725 Jenkyns, H.C. (2010), Geochemistry of oceanic anoxic events. *Geochemistry*,
726 *Geophysics, Geosystems*, **11**, Q03004, doi:10.1029/2009GC002788.

727

728 John, S. G., & Conway, T. M. (2014). A role for scavenging in the marine
729 biogeochemical cycling of zinc and zinc isotopes. *Earth and Planetary Science*
730 *Letters*, **394**, 159–167.

731

732 John, S. G., Kunzmann, M., Townsend, E. J., & Rosenberg, A. D. (2017). Zinc and
733 cadmium stable isotopes in the geological record: A case study from the post-
734 snowball Earth Nuccaleena cap dolostone. *Palaeogeography, Palaeoclimatology*,
735 *Palaeoecology*, **466**, 202–208.

736

737 John, S. G., Helgoe, J., & Townsend, E. (2018). Biogeochemical cycling of Zn and Cd
738 and their stable isotopes in the Eastern Tropical South Pacific. *Marine Chemistry*,
739 **201**, 256–262.

740

741 Joo, Y.J. & Sageman, B.B. (2014) Cenomanian to Campanian carbon isotope
742 chemostratigraphy from the Western Interior Basin, USA. *Journal of Sedimentary*
743 *Research*, **84**, 529–542.

744

745 Lane, T. W., Saito, M. A., George, G. N., Pickering, I. J., Prince, R. C., & Morel, F. M.
746 (2005). Biochemistry: a cadmium enzyme from a marine diatom. *Nature*, **435**,
747 42–42.

748

749 Lacan, F., Francois, R., Ji, Y., & Sherrell, R. M. (2006). Cadmium isotopic
750 composition in the ocean. *Geochimica et cosmochimica acta*, **70**(20), 5104–5118.

751

752 Little, S.H., Chen, L., Kreissig, K., Severmann, S., & McManus, J., 2019. Isotopically
753 Light Cd in Sediments Underlying Oxygen Deficient Zones. *Goldschmidt 2019*
754 *conference abstract*.

755

756 Little, S. H., Vance, D., Lyons, T. W., & McManus, J. (2015). Controls on trace metal
757 authigenic enrichment in reducing sediments: insights from modern oxygen-
758 deficient settings. *American Journal of Science*, **315**(2), 77–119.

759

Minisini, D., Eldrett, J.S., Bergman, S.C. and Forkner, R. (2018),
Chronostratigraphic framework and depositional environments in the organic-
rich, mudstone-dominated Eagle Ford Group, Texas, USA. *Sedimentology*, **65**,
1520–1557.

Middag, R., van Heuven, S. M., Bruland, K. W., & de Baar, H. J. (2018). The
relationship between cadmium and phosphate in the Atlantic Ocean unravelled.
Earth and Planetary Science Letters, **492**, 79-88.

Morel, F. M. (2013). The oceanic cadmium cycle: Biological mistake or
utilization? *Proceedings of the National Academy of Sciences*, **110** (21), E1877–
E1877.

Morford, J. L., & Emerson, S. (1999). The geochemistry of redox sensitive trace
metals in sediments. *Geochimica et Cosmochimica Acta*, **63**(11-12), 1735–1750.

Owens, J.D., Reinhard, C.T., Rohressen, M., Love, G.L. and Lyons, T.W. (2016),
Empirical links between trace metal cycling and marine microbial ecology during
a large perturbation to Earth's carbon cycle. *Earth and Planetary Science Letters*,
449, 407–417.

Pearce, C. R., Cohen, A. S., & Parkinson, I. J. (2009). Quantitative separation of
molybdenum and rhenium from geological materials for isotopic determination
by MC - ICP - MS. *Geostandards and Geoanalytical Research*, **33**(2), 219-229.

785 Quay, P., Cullen, J., Landing, W., & Morton, P. (2015). Processes controlling the
786 distributions of Cd and PO₄ in the ocean. *Global Biogeochemical Cycles*, **29**, 830–
787 841.

788

789 Ripperger, S., Rehkämper, M., Porcelli, D., & Halliday, A.N. (2007). Cadmium
790 isotope fractionation in seawater—a signature of biological activity. *Earth and*
791 *Planetary Science Letters*, **261**, 670–684.

792

793 Rosenthal, Y., Lam, P., Boyle, E. A., & Thomson, J. (1995). Authigenic cadmium
794 enrichments in suboxic sediments: Precipitation and postdepositional mobility.
795 *Earth and Planetary Science Letters*, **132**(1-4), 99–111.

796

797 Rudnick, R.L. and S. Gao (2003), Composition of the continental crust. *Treatise on*
798 *Geochemistry*, 1–64.

799

800 Scaife, J. D., Ruhl, M., Dickson, A. J., Mather, T. A., Jenkyns, H. C., Percival, L. M. E., ...
801 & Minisini, D. (2017). Sedimentary mercury enrichments as a marker for
802 submarine large igneous province volcanism? Evidence from the Mid -
803 Cenomanian event and Oceanic Anoxic Event 2 (Late Cretaceous). *Geochemistry,*
804 *Geophysics, Geosystems*, **18**(12), 4253–4275.

805

806 Schlanger, S. O. & Jenkyns, H. (1976). Cretaceous oceanic anoxic events: causes
807 and consequences. *Geologie en Mijnbouw*, **55**, 179–184.

808

809 Scholle, P. A. & Arthur, M. A. (1980). Carbon isotope fluctuations in cretaceous
810 pelagic limestones: potential stratigraphic and petroleum exploration tool. *AAPG*
811 *Bulletin*, **64**, 67–87.

812

813 Schlanger, S.O., Arthur, M.A., Jenkyns, H.C. and Scholle, P.A. (1987), The
814 Cenomanian–Turonian oceanic anoxic event, I: stratigraphy and distribution of
815 organic carbon-rich beds and the marine $\delta^{13}\text{C}$ excursion. *Marine Petroleum*
816 *Source Rocks*, Geological Society of London Special Publication, **26**, 371–399.

817

818 Scott, C. & Lyons, T. W. (2012). Contrasting molybdenum cycling and isotopic
819 properties in euxinic versus non-euxinic sediments and sedimentary rocks:
820 Refining the paleoproxies. *Chemical Geology*, **324**, 19–27.

821

822 Sieber, M., Conway, T. M., de Souza, G. F., Obata, H., Takano, S., Sohrin, Y., & Vance,
823 D. (2019). Physical and biogeochemical controls on the distribution of dissolved
824 cadmium and its isotopes in the Southwest Pacific Ocean. *Chemical Geology*, **511**,
825 494–509.

826

827 Sun, X., Zhang, T., Milliken, K.L. and Sun, D. (2016), Geochemical evidence for
828 organic matter source input and depositional environments in the lower and
829 upper Eagle Ford Group, south Texas. *Organic Geochemistry*, **98**, 66–81.

830

831 Tankere, S., Muller, F., Burton, J., Statham, P., Guieu, C., & Martin, J.-M. (2001).
832 Trace metal distributions in shelf waters of the northwestern Black Sea.
833 *Continental Shelf Research*, **21**, 1501–1532.

834

835 Tsikos, H., Jenkyns, H.C., Walsworth-Bell, B., Petrizzo, M.R., Forster, A., Kolonic, S.,
836 Erba, E., Premoli Silva, I., Baas, M., Wagner, T. and Sinninghe Damsté, J.S. (2004),
837 Carbon-isotope stratigraphy recorded by the Cenomanian–Turonian Oceanic
838 Anoxic Event: correlation and implications based on three key localities. *Journal*
839 *of the Geology Society of London*, **161**, 711–719.

840

841 Vance, D., Little, S. H., Archer, C., Cameron, V., Andersen, M. B., Rijkenberg, M. J., &
842 Lyons, T. W. (2016). The oceanic budgets of nickel and zinc isotopes: the
843 importance of sulfidic environments as illustrated by the Black Sea. *Philosophical*
844 *Transactions of the Royal Society A: Mathematical, Physical and Engineering*
845 *Sciences*, **374**(2081), 20150294.

846

847 Xie, R. C., Galer, S. J., Abouchami, W., Rijkenberg, M. J., De Baar, H. J., De Jong, J., &
848 Andreae, M. O. (2017). Non-Rayleigh control of upper-ocean Cd isotope
849 fractionation in the western South Atlantic. *Earth and planetary science letters*,
850 **471**, 94–103.

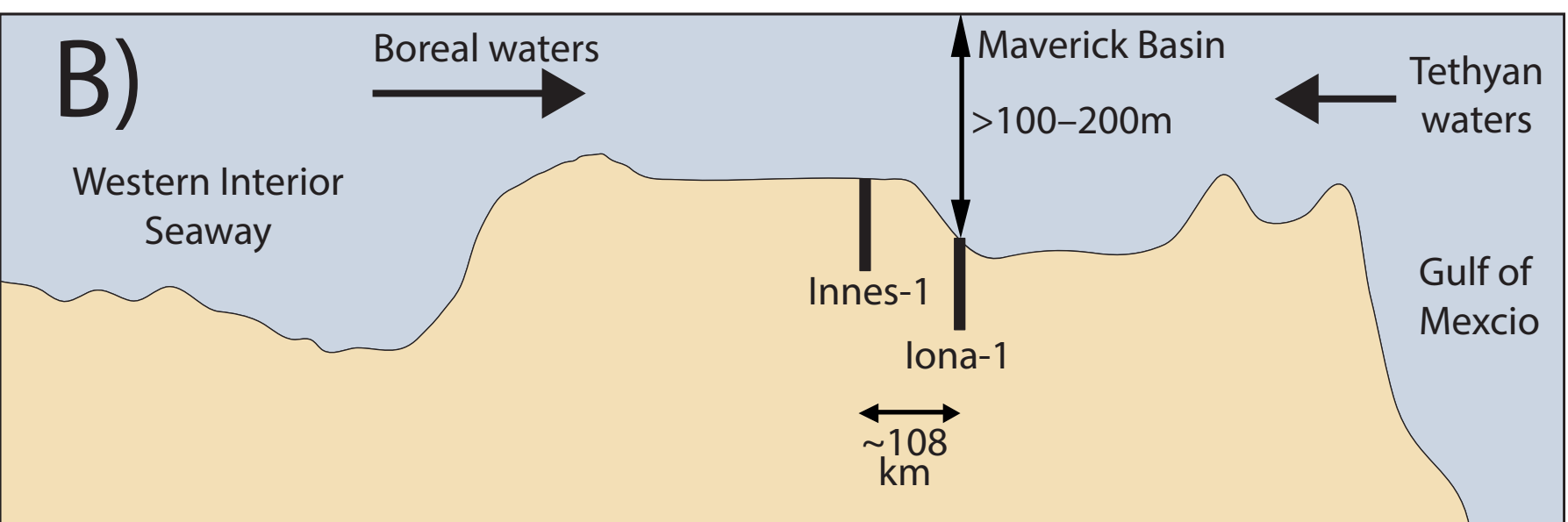
851

852 Xie, R. C., Rehkämper, M., Grasse, P., van de Flierdt, T., Frank, M., & Xue, Z. (2019).
853 Isotopic evidence for complex biogeochemical cycling of Cd in the eastern
854 tropical South Pacific. *Earth and Planetary Science Letters*, **512**, 134–146.

855

856 Xue, Z., Rehkämper, M., Horner, T. J., Abouchami, W., Middag, R., van de Flierdt, T.,
857 & de Baar, H. J. (2013). Cadmium isotope variations in the Southern Ocean. *Earth*
858 *and Planetary Science Letters*, **382**, 161–172.

Figure 1



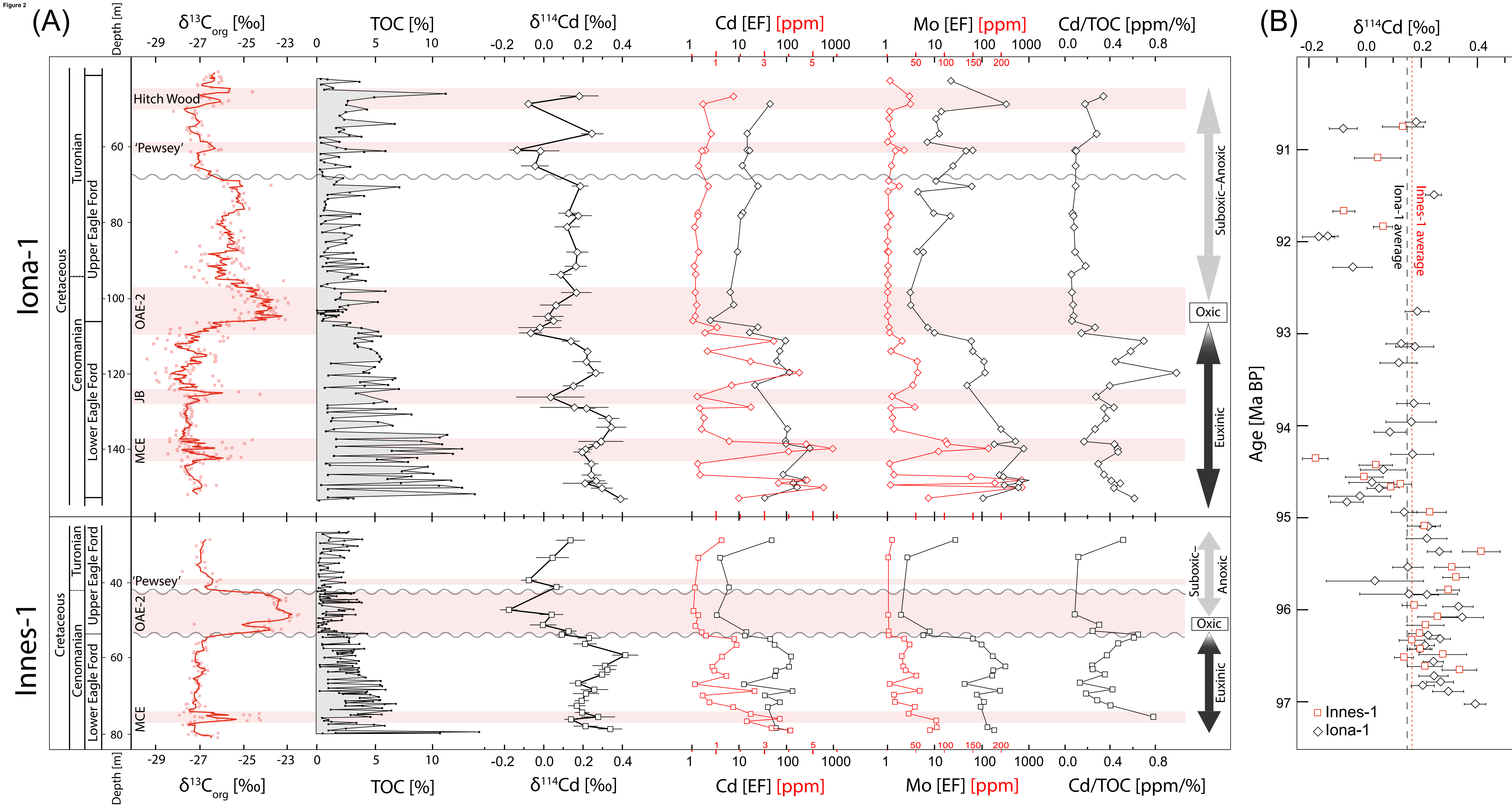


Figure 3

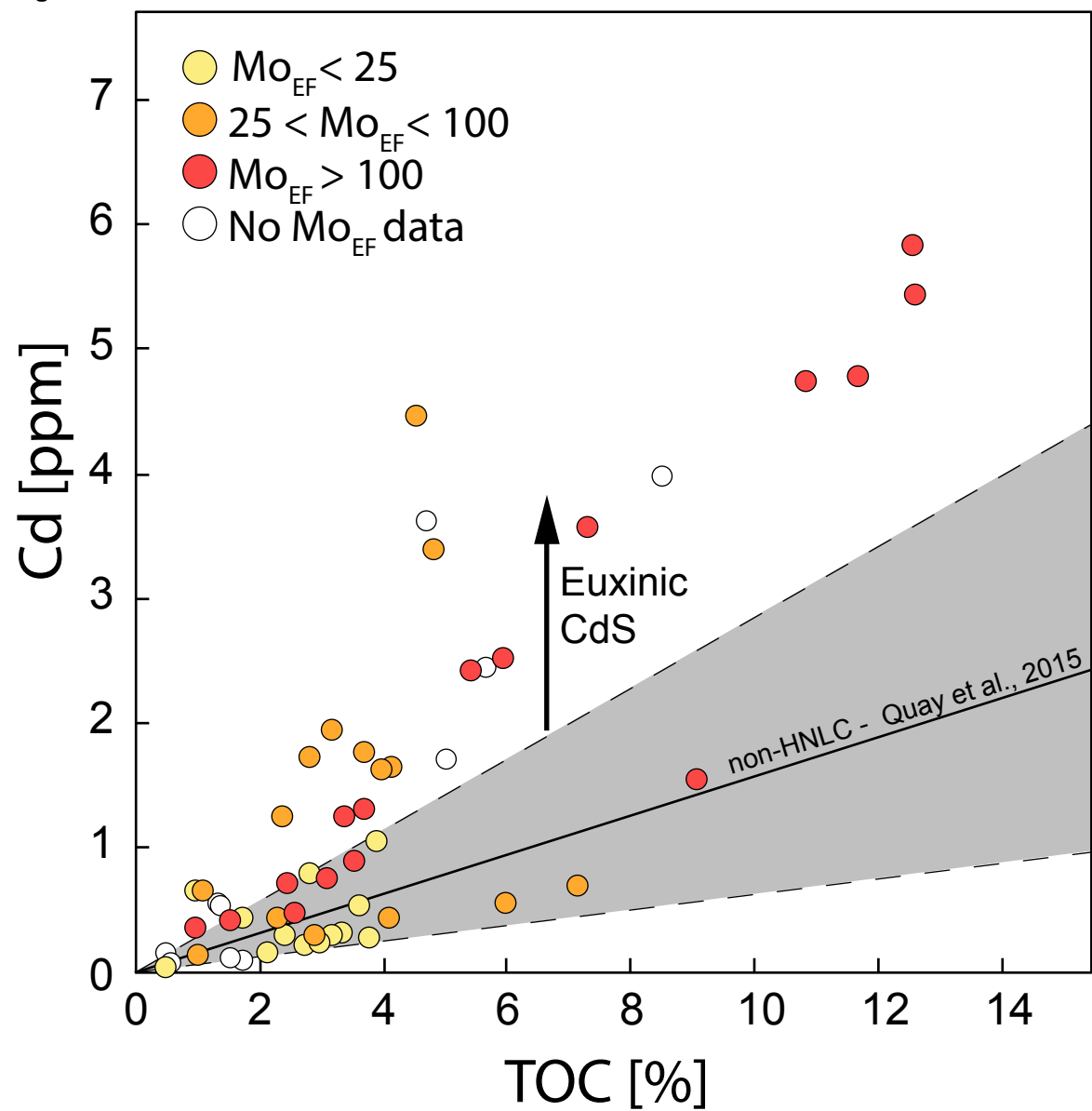
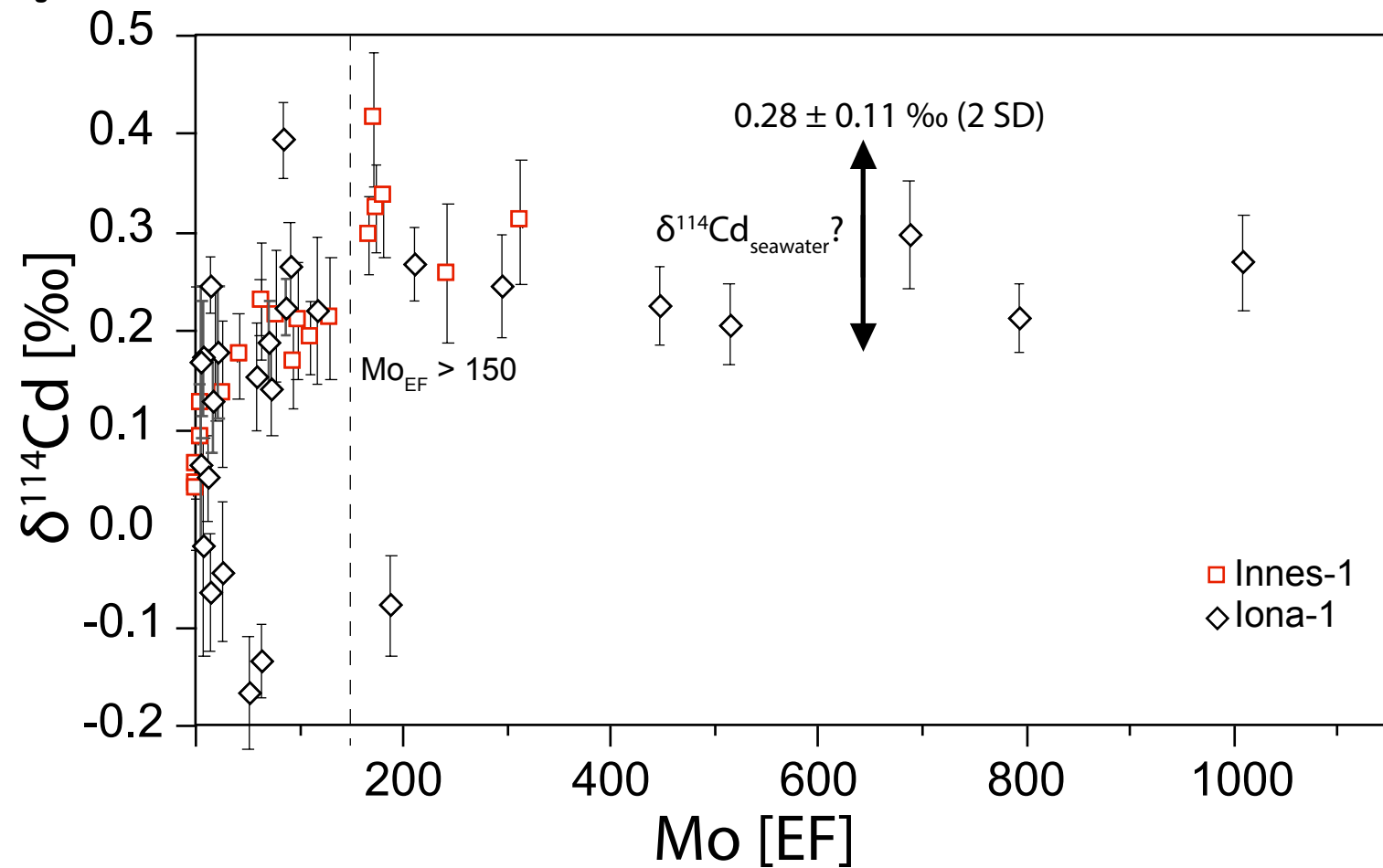


Figure 4



Non-euxinic conditions

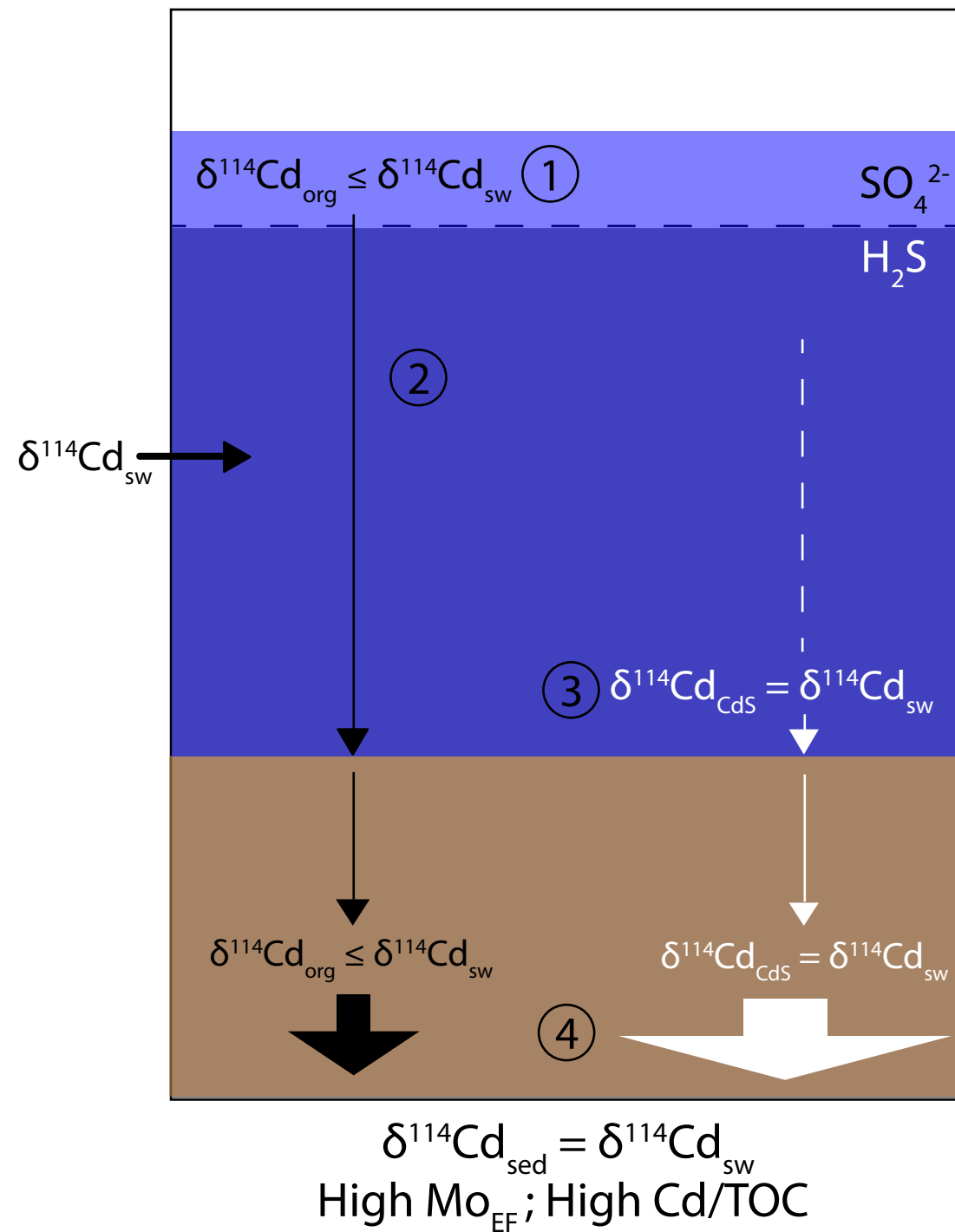


Figure 6

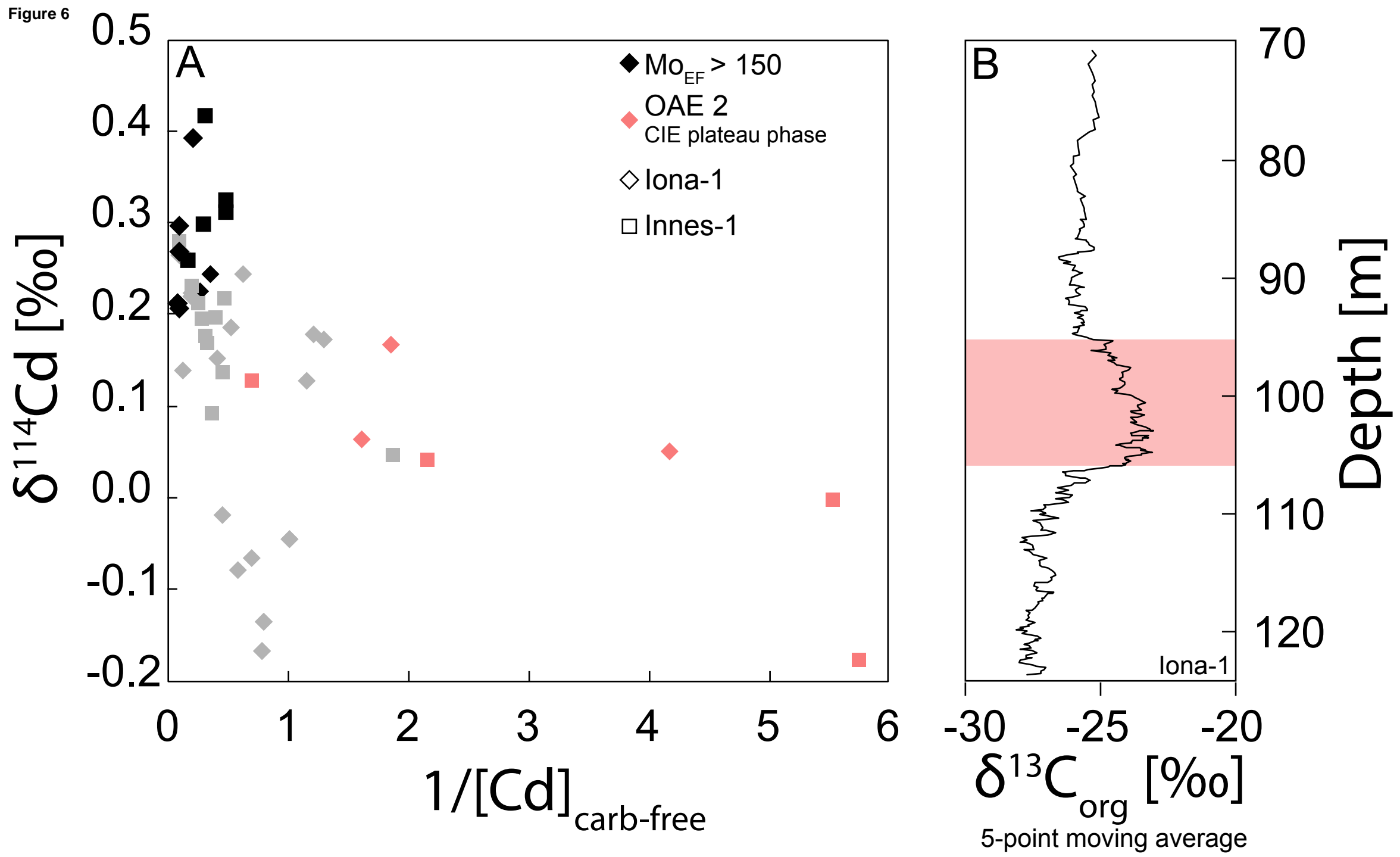


Figure 7

